# Analyzing Power Correlation Distributions for Dynamic Spectrum Awareness in 5G Networks

Andrew Ashdown<sup>†,+</sup>, John Kelly<sup>\*</sup>, Jonathan Ashdown<sup>\*</sup>, Ian Kurzrock<sup>†</sup>, Caden Turck<sup>†</sup>, and Francesco Restuccia<sup>+</sup>

<sup>+</sup>Institute for the Wireless Internet of Things, Northeastern University, United States

<sup>\*</sup>Air Force Research Laboratory, United States

<sup>†</sup>Radiance Technologies, United States

Abstract-With continued advancements in the cellular domain, the number of network devices is expanding rapidly. Furthermore, as devices become smarter and more advanced with the deployment of dynamic spectrum awareness techniques that facilitate increased spectral efficiency, developing robust methodologies to analyze limited spectrum resources will be crucial to the success of FutureG wireless communications. Central to the idea of dynamic spectrum awareness is the need for robust techniques and metrics that provide insight into the spectral utilization and can be harnessed by dynamic control loops to maximize spectral usage and eliminate wasteful inefficiencies. While a plethora of dynamic spectrum awareness tactics have been proposed, existing strategies do not analyze the power spectral density probability distribution across time, which we demonstrate is a relevant indicator of spectral usage and signal quality. Specifically, we harness the commercialgrade, standalone, 5G network architecture located at the Air Force Research Laboratory (AFRL) to perform an experimental measurement study and show the effectiveness of representing the localized spectral utilization as a distribution of power correlations w.r.t. the bandwidth's frequency bins. We analyze the distributional structure of power spectral density correlations for a variety of wireless channel environments (i.e., LOS, NLOS, and Edge scenarios) and locations, and our key finding is that the shape of the frequency-bin correlation distribution changes significantly depending upon the particular wireless channel situation. As such, our approach - which is not only blind (i.e., it doesn't require knowledge about the signal prior to sensing the spectrum), but also highly practical from an implementation standpoint - provides fresh insight into the spectral utilization, signal structure, and channel quality conditions.

#### I. INTRODUCTION

Recent advances in cellular communications [1] have caused the number of mobile connections to increase significantly. One study predicted that by 2025 the number of mobile devices worldwide will exceed 18 billion [2]. As such, the inherently scarce sub-6 GHz spectrum is becoming increasingly overcrowded and underutilized [3] [4]. Researchers and industry alike [5] [6] are working to make mobile devices smarter and more spectrum-efficient, particularly with the rise of fifth generation cellular networks (5G) and the Internet of Things which are bringing in unprecedented device counts that must be matched by equal advances in device capabilities [4]. For instance, a new effort proposed by Restuccia *et al.* motivates the need for data-driven solutions to address the spectrum crunch [7]. They propose a system level architecture which is based upon the principles of Open Radio Access

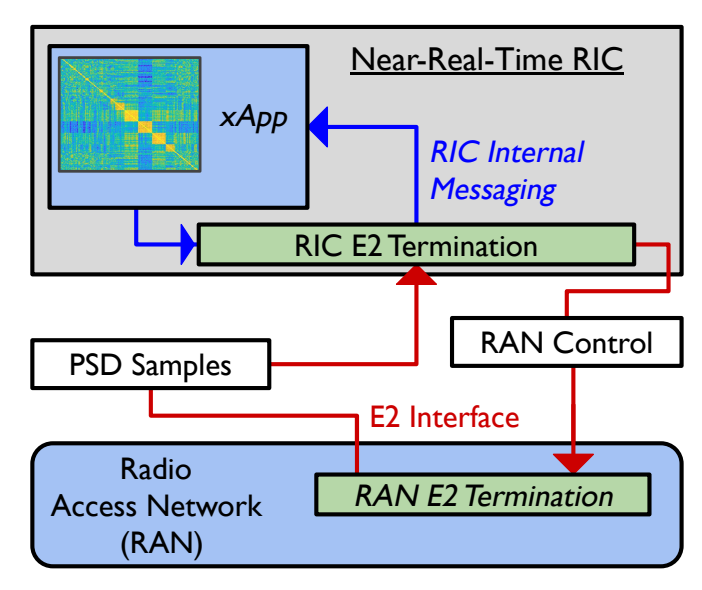


Fig. 1: An Example Integration of our Spectrum Sensing Approach with the O-RAN Architecture.

Networks (Open RAN) [8], [9], dynamic data-driven control loops [10]–[13], and robust spectrum awareness techniques [14]. This architecture and related dynamic spectrum awareness strategies will radically transform the current cellular landscape and introduce previously unseen spectral efficiency into the 5G ecosystem.

With this in mind, we pursue a fresh technique to monitor sub-6 GHz spectral utilization and channel quality in the 5G landscape. Figure 1 provides an example of how our approach could be integrated with the Open RAN system architecture as a source of spectral information to data-driven, Artificial Intelligence (AI)-based control structures housed inside the Near-Real-Time-RIC [7]. As shown in Figure 1, the Radio Access Network (RAN) would collect and send power spectral density (PSD) samples to the Near-Real-Time-RIC via the E2 Interface. To collect the PSD measurements in this study we used a simple horn antenna attached to a handheld spectrum analyzer – in practice, any power level measurement collected at the RAN would suffice. The Near-Real-Time-RIC then transfers the PSD samples to a dedicated containerized xApp located within the Near-Real-Time-RIC. xApps are at the center of the Open RAN revolution as they house the AI models that the Near-Real-Time-RIC uses to control the RAN [8] [9]. In our case, the xApp would perform the correlation

analysis – see Section IV – and provide spectral insight which could then be transferred to the Near-Real-Time-RIC for dynamic RAN control, or logged for explainability.

## Summary of Novel Contributions

In this work, we present a fresh technique for dynamic spectrum awareness (particularly in the 5G landscape). Our approach is blind, which means that it requires zero a priori information about the signal or wireless channel. Specifically, our strategy is to analyze the PSD frequency bin correlation probability distribution to gain insight into the localized spectral structure as it varies over time. We show that the shape of the correlation distribution is directly related to the signal characteristics and channel quality. We observe that the signal structure induces a highly correlated block diagonal in the frequency bin correlation matrix when the wireless channel is relatively unobstructed. This block diagonal in turn causes a multimodal structure in the probability density function (PDF) due to the high-correlation clusters. Thus, the key finding is that the structure of the correlation matrix, and thus the shape of the correlation distribution, change in accordance with the wireless channel condition. This implies that the shape of the PSD frequency bin correlation distribution can be analyzed to monitor the 5G signal/channel characteristics. In addition to our in-the-field experiments using Air Force Research Laboratory (AFRL)'s testbed, we also perform simulation experiments using the MATLAB 5G Toolbox [15] to verify our results and confirm our discoveries. To the best of our knowledge, this distributional technique has not been explored previously for dynamic spectrum awareness.

The remainder of our paper is divided as follows: Section III outlines related work. Section III provides an overview of AFRL's 5G testbed located in Stockbridge, New York [16]. Section IV details our experimental setup, data analysis, results, and an explanation of our findings. Section V concludes our work and outlines extensions we plan to pursue in collaboration with AFRL.

#### II. RELATED WORK

Many techniques related to the concept of dynamic spectrum awareness/sensing/access have been proposed over the years and there are a plethora of helpful surveys covering these topics [17] [18]. However, techniques that are closest to our approach are those which correlate the power spectral density frequency bins (e.g., [19] [20]), since we are also performing this operation. However, while it is not novel to correlate PSD frequency bins, we have not seen another work that analyzes the probability distribution of the correlation matrix with the goal of harnessing known distribution analysis techniques for dynamic spectral awareness. Existing techniques analyze the correlation matrix as a heatmap (which we do as well), but our distributional approach seems to be uninvestigated.

# III. TESTBED AND EXPERIMENTAL OVERVIEW

We used a commercial-grade 5G cellular network located at the 300 acre test facility operated by AFRL in Stockbridge,

New York [16]. A high-level overview of the system architecture is shown in Figure 2. As shown, a User Interface (UI) gives the operator control of various network functionalities. Two primary control capabilities are the Physical Resource Block (PRB) blanking and beam muting applications. The PRB blanking functionality allows designated portions of the network bandwidth to be "blanked" or essentially "turned off" upon operator command. The beam muting operation provides flexibility in the beam configuration which allows specified beams to be "muted" for various situations. During the course of our experiments, we utilized the PRB blanking functionality to downsize the bandwidth from its 100MHz default setting. Figure 2 also shows a turntable upon which a gNodeB (gNB) is mounted for convenient rotation. While there are others on site, this was the primary gNB that we utilized for our experiments.

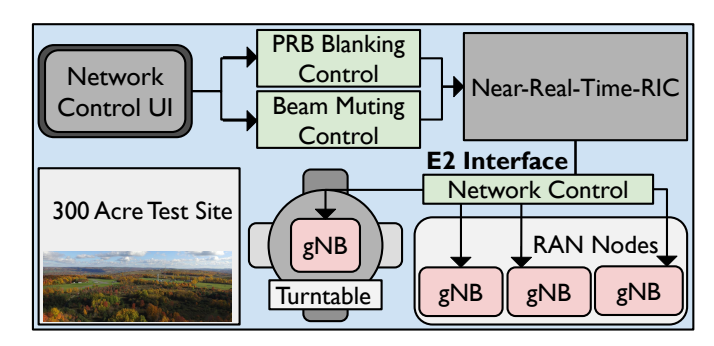


Fig. 2: AFRL's 5G Testbed in Stockbridge, New York [16].



Fig. 3: Experimental Setup for LOS, Edge, and NLOS Wireless Channel Situations [21].

# Experimental Setup

The gNB we utilized for our experiments was placed in an Artificial Loading mode to replicate User Equipment (UE) connectivity. This way, the gNB pseudo-randomly selects time and frequency resources in which to transmit and behaves as if it were serving a large number of UEs. Next, we utilized the existing terrain to capture the signal behavior in Line-of-Sight (LOS), Edge, and Non-Line-of-Sight (NLOS) wireless channel conditions. We were particularly interested to observe the transition from LOS to NLOS. Figure 3 shows our experimental setup in which we used a large concrete block located on site as a signal obstruction and collected PSD measurements for each of the three channel types using a simple horn antenna attached to a handheld spectrum analyzer. We performed twenty separate collections for each of the three channel types, where each collection represented an average of the last five hundred PSD measurements over a total of 401 frequency bins (which was the default) from 3.36GHz to 3.39GHz (an arbitrary frequency range in the network's supported 5G band). We were able to perform this experiment at two different locations on site by utilizing two different concrete blocks that were separated from each other by about five hundred feet, but comparable in their distances from the gNB; we denote these two experimental locations as Scenario 1 and Scenario 2, respectively. This allowed us to compare the LOS, Edge, and NLOS results for each scenario.

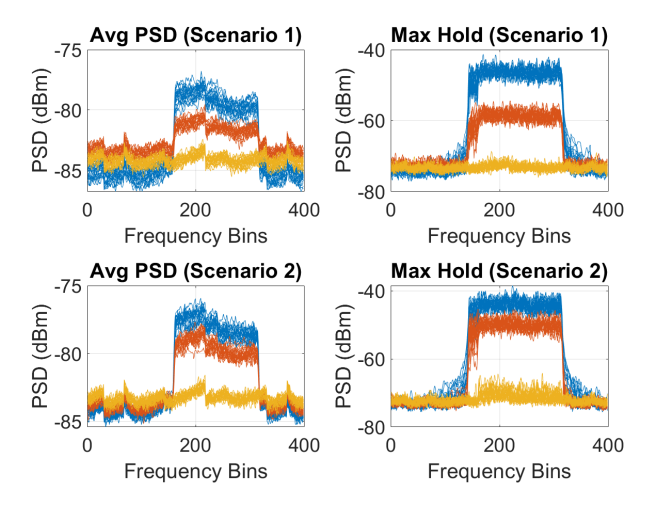


Fig. 4: Average Power Spectral Density and Max Hold for 20 Collections Spanning 3.36GHz - 3.39GHz (Blue: LOS, Red: Edge, Yellow: NLOS).

#### IV. EXPERIMENTAL RESULTS

Figure 4 shows the average PSD collected at the two measurement locations, as well as the respective Max Hold plots (which record the max power at each frequency bin). Each of the graphs consist of sixty time series PSD (or Max Hold) plots where the twenty blue plots represent the LOS collections, the twenty red represent the Edge collections, and the twenty yellow represent the NLOS collections. The x-axis denotes the respective frequency bins into which the observed bandwidth was divided at reception (i.e., in the handheld spectrum analyzer); in our case we used the handheld spectrum analyzer's default setting which was 401 frequency bins. As expected, there is a clear transition in the average and maximum PSD magnitudes as the receiver was moved from the LOS to the NLOS condition.

Upon collecting twenty PSD measurements for each of the three wireless channel conditions (and at the two separate locations) we then correlated the power level of each PSD frequency bin across the twenty collections using (1).

$$\rho(b_x, b_y) = \frac{1}{C - 1} \sum_{i=1}^{C} \frac{b_x^i - \bar{b_x}}{\sigma_x} \frac{b_y^i - \bar{b_y}}{\sigma_y}$$
(1)

In this equation C represents the number of collections (20 in our case) and  $b_x$  and  $b_y$  represent the frequency bins being correlated. Thus, in total we correlated all frequency bins between 3.36GHz and 3.39GHz (the bandwidth we chose to

observe) and analyzed the relationship that individual frequencies have with one another inside the bandwidth of interest. Upon completing the correlation analysis we obtained a matrix of the form, M from (2), for each channel condition/location pair. Since we had 401 frequency bins, N was equal to 401.

$$M = \begin{bmatrix} \rho(b_1,b_1) & \cdots & \rho(b_1,b_N) \\ \rho(b_N,b_1) & \cdots & \rho(b_N,b_N) \end{bmatrix}$$

$$\begin{bmatrix} \mathbf{Scenario 1: LOS} \\ 100 \\ 200 \\ 0 \end{bmatrix} \begin{bmatrix} \mathbf{Scenario 1: LOS} \\ 100 \\ 200 \\ 0 \end{bmatrix} \begin{bmatrix} \mathbf{Scenario 2: LOS} \\ 100 \\ 200 \\ 0 \end{bmatrix} \begin{bmatrix} \mathbf{Scenario 2: LOS} \\ 100 \\ 200 \\ 0 \end{bmatrix} \begin{bmatrix} \mathbf{Scenario 2: LOS} \\ 100 \\ 200 \\ 0 \end{bmatrix} \begin{bmatrix} \mathbf{Scenario 2: LOS} \\ 100 \\ 200 \\ 0 \end{bmatrix} \begin{bmatrix} \mathbf{Scenario 2: LOS} \\ 100 \\ 200 \\ 0 \end{bmatrix} \begin{bmatrix} \mathbf{Scenario 2: LOS} \\ 100 \\ 200 \\ 0 \end{bmatrix} \begin{bmatrix} \mathbf{Scenario 2: LOS} \\ 100 \\ 200 \\ 0 \end{bmatrix} \begin{bmatrix} \mathbf{Scenario 2: LOS} \\ 100 \\ 200 \\ 0 \end{bmatrix} \begin{bmatrix} \mathbf{Scenario 2: LOS} \\ 100 \\ 200 \\ 0 \end{bmatrix} \begin{bmatrix} \mathbf{Scenario 2: LOS} \\ 100 \\ 200 \\ 0 \end{bmatrix} \begin{bmatrix} \mathbf{Scenario 2: LOS} \\ 100 \\ 200 \\ 0 \end{bmatrix} \begin{bmatrix} \mathbf{Scenario 2: LOS} \\ 100 \\ 200 \\ 0 \end{bmatrix} \begin{bmatrix} \mathbf{Scenario 2: LOS} \\ 100 \\ 200 \\ 0 \end{bmatrix} \begin{bmatrix} \mathbf{Scenario 2: LOS} \\ 100 \\ 200 \\ 0 \end{bmatrix} \begin{bmatrix} \mathbf{Scenario 2: LOS} \\ 100 \\ 200 \\ 0 \end{bmatrix} \begin{bmatrix} \mathbf{Scenario 2: LOS} \\ 100 \\ 200 \\ 0 \end{bmatrix} \begin{bmatrix} \mathbf{Scenario 2: LOS} \\ 100 \\ 200 \\ 0 \end{bmatrix} \begin{bmatrix} \mathbf{Scenario 2: LOS} \\ 100 \\ 200 \\ 0 \end{bmatrix} \begin{bmatrix} \mathbf{Scenario 2: LOS} \\ 100 \\ 200 \\ 0 \end{bmatrix} \begin{bmatrix} \mathbf{Scenario 2: LOS} \\ 100 \\ 200 \\ 0 \end{bmatrix} \begin{bmatrix} \mathbf{Scenario 2: LOS} \\ 100 \\ 200 \\ 0 \end{bmatrix} \begin{bmatrix} \mathbf{Scenario 2: LOS} \\ 100 \\ 200 \\ 0 \end{bmatrix} \begin{bmatrix} \mathbf{Scenario 2: LOS} \\ 100 \\ 200 \\ 0 \end{bmatrix} \begin{bmatrix} \mathbf{Scenario 2: LOS} \\ 100 \\ 200 \\ 0 \end{bmatrix} \begin{bmatrix} \mathbf{Scenario 2: LOS} \\ 100 \\ 200 \\ 0 \end{bmatrix} \begin{bmatrix} \mathbf{Scenario 2: LOS} \\ 100 \\ 200 \\ 0 \end{bmatrix} \begin{bmatrix} \mathbf{Scenario 2: LOS} \\ 100 \\ 200 \\ 0 \end{bmatrix} \begin{bmatrix} \mathbf{Scenario 2: LOS} \\ 100 \\ 200 \\ 0 \end{bmatrix} \begin{bmatrix} \mathbf{Scenario 2: LOS} \\ 100 \\ 200 \\ 0 \end{bmatrix} \begin{bmatrix} \mathbf{Scenario 2: LOS} \\ 100 \\ 200 \\ 0 \end{bmatrix} \begin{bmatrix} \mathbf{Scenario 2: LOS} \\ 100 \\ 200 \\ 0 \end{bmatrix} \begin{bmatrix} \mathbf{Scenario 2: LOS} \\ 100 \\ 200 \\ 0 \end{bmatrix} \begin{bmatrix} \mathbf{Scenario 2: LOS} \\ 100 \\ 200 \\ 0 \end{bmatrix} \begin{bmatrix} \mathbf{Scenario 2: LOS} \\ 100 \\ 200 \\ 0 \end{bmatrix} \begin{bmatrix} \mathbf{Scenario 2: LOS} \\ 100 \\ 200 \\ 0 \end{bmatrix} \begin{bmatrix} \mathbf{Scenario 2: LOS} \\ 100 \\ 200 \\ 0 \end{bmatrix} \begin{bmatrix} \mathbf{Scenario 2: LOS} \\ 100 \\ 200 \\ 0 \end{bmatrix} \begin{bmatrix} \mathbf{Scenario 2: LOS} \\ 100 \\ 200 \\ 0 \end{bmatrix} \begin{bmatrix} \mathbf{Scenario 2: LOS} \\ 100 \\ 200 \\ 0 \end{bmatrix} \begin{bmatrix} \mathbf{Scenario 2: LOS} \\ 100 \\ 200 \\ 0 \end{bmatrix} \begin{bmatrix} \mathbf{Scenario 2: LOS} \\ 100 \\ 200 \\ 0 \end{bmatrix} \begin{bmatrix} \mathbf{Scenario 2: LOS} \\ 100 \\ 200 \\ 0 \end{bmatrix} \begin{bmatrix} \mathbf{Scenario 2: LOS} \\ 100 \\ 200 \\ 0 \end{bmatrix} \begin{bmatrix} \mathbf{Scenario 2: LOS} \\ 100 \\ 200 \\ 0 \end{bmatrix} \begin{bmatrix} \mathbf{Scenario 2: LOS} \\ 100 \\ 200 \\ 0 \end{bmatrix} \begin{bmatrix} \mathbf{Scenario 2: LOS} \\ 100 \\ 200 \\ 0 \end{bmatrix} \begin{bmatrix} \mathbf{Scenario 2: LOS} \\ 100 \\ 200 \\ 0 \end{bmatrix} \begin{bmatrix} \mathbf{Scenario 2: LOS} \\ 100 \\ 200 \\ 0 \end{bmatrix} \begin{bmatrix} \mathbf{Scenario 2: LOS} \\ 10$$

Fig. 5: Frequency Bin Correlations of Average Power Spectral Density Spanning 3.36GHz - 3.39GHz for LOS, Edge, and NLOS Wireless Channel Cases.

100 200 300

Frequency Bins

100 200 300

Frequency Bins

Figure 5 displays heatmap representations for each of these correlation matrices. It is noteworthy that the average PSD LOS cases exhibit a strong block diagonal structure at each of the two collection locations; we will discuss the explanation for this phenomenon shortly. Furthermore, we notice a clear fading of the block diagonal as the channel condition moves from Edge to NLOS.

A related phenomenon we observed upon analyzing the PDF distribution of the frequency bin correlation matrices is that the shape of the distribution changes in accordance with the wireless channel situation. As shown in Figure 6 (which represents the PDF for each of the matrices in Figure 5), the distributions representing the LOS case are significantly different from those of the NLOS case, while the Edge case falls somewhere in between the two. Specifically, in Figure 6

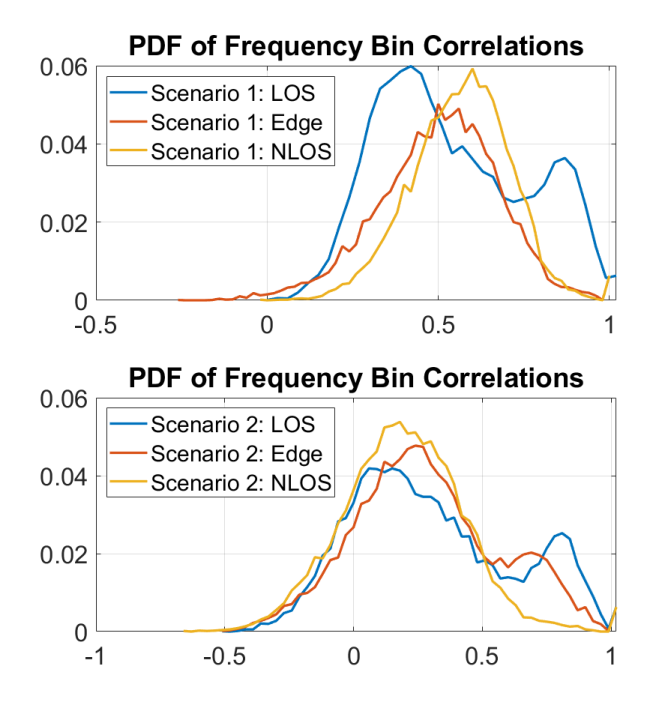


Fig. 6: Probability Density Functions of Average Power Spectral Density frequency bin Correlations.

the LOS cases exhibits a clear bimodal structure; this feature is much less distinct in the Edge cases, and noticeably absent in the NLOS cases. It should be mentioned that to generate the distributions shown in Figure 6 the left and right-hand sides of the collected bandwidth were trimmed such that we were only correlating the frequency bins with signal power (this does not violate the claim to be a blind technique since after blindly collecting the measurements it is clear from both the time series plots in Figure 4 and the location of the block diagonal in Figure 5 where the signal power is located).

## Explanation of Experimental Findings

The reason behind the block diagonal structure in the LOS and Edge correlation matrices and the corresponding multimodal PDFs is not particularly obvious. At first glance, one may suppose that the block diagonal is caused by the windowing overlap introduced by the Fast Fourier Transform in the handheld spectrum analyzer. However, because we are not correlating w.r.t. time but rather frequency, this is clearly not the case. Furthermore, the strength and well-defined nature of the block diagonal clearly eliminates the possibility that this is a natural phenomenon induced by the wireless channel itself. If this were the case we would expect smearing in the block diagonal structure rather than the clear-cut characteristics we observe in Figure 5. Additionally, the absence of the block diagonal structure in the NLOS case indicates that this is not caused at the receiver side in the handheld spectrum analyzer. Rather, our intuition is that it must be a characteristic of the signal generated by the transmitter (the gNB in this case). This seems to be the only logical reason for a well-defined block diagonal structure in the LOS frequency bin correlation matrix that is completely absent from the corresponding NLOS frequency bin correlation matrix.

Additionally, the bimodal shape of the LOS distributions in Figure 6 seems to be caused by the signal structure as well. Our intuition is that it is not caused by multi-path (since there were not many reflectors near our experimental setup), but rather is explained by the existence of pockets of high correlation amidst swaths of low correlation in the correlation matrices. Given these observations, it then follows that through our correlative analysis we are given a glimpse into the structural characteristics of the signal. After validating our intuitions through 1) additional in-the-field experiments designed to establish a measurement baseline, and 2) software-based simulations that replicated the 5G signal reception, we will explore the significance of these results in the context of dynamic spectrum awareness.

Validation of Experimental Explanations

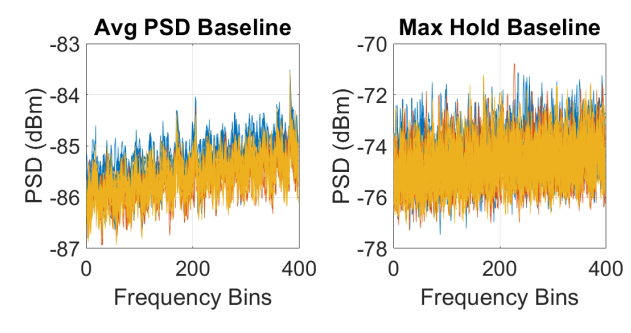


Fig. 7: Baseline Average Power Spectral Density and Max Hold for Scenario 1 (Blue: LOS (20 collections), Red: Edge (13 collections), Yellow: NLOS (20 collections)).

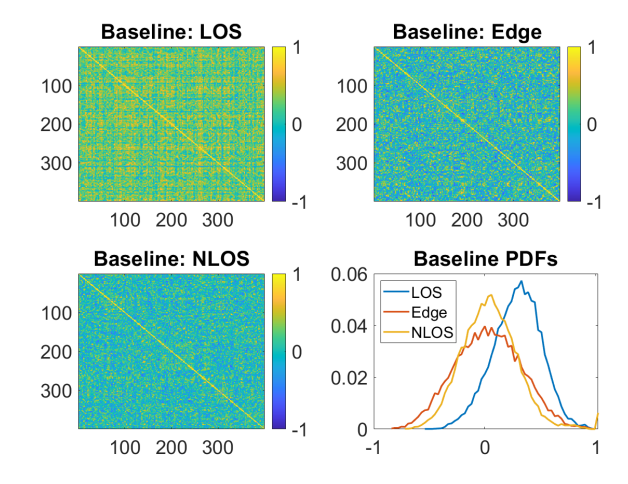


Fig. 8: Baseline frequency bin Correlation Matrices and Distributions.

The primary distinction between the in-the-field baseline collections and our previous experiments is that we powered off the gNB prior to collecting the baseline data, thus removing the effects of the 5G signal. Figure 7 shows the time series representation of these collections for the LOS, Edge, and

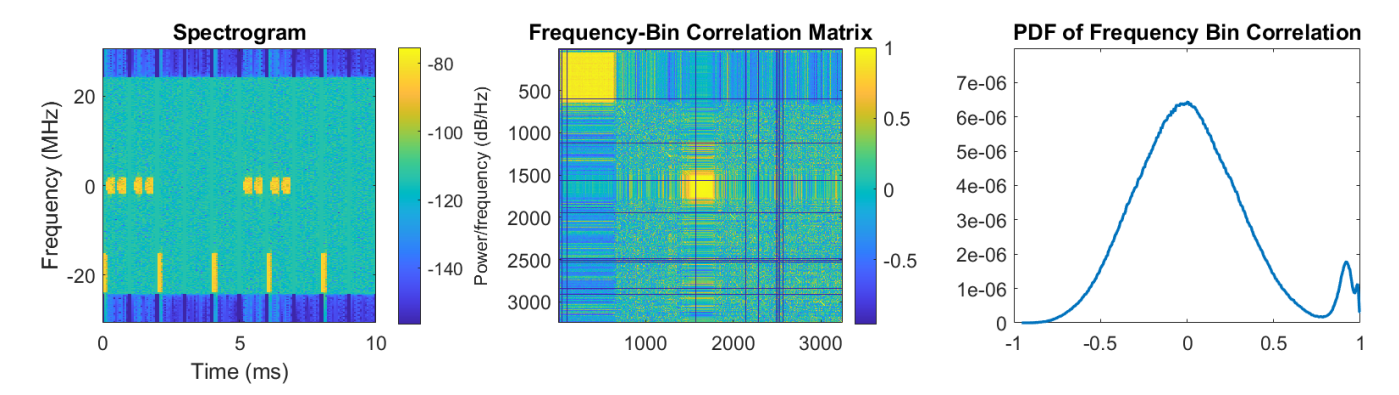


Fig. 9: MATLAB Simulations to Validate In-The-Field Experimental Findings.

NLOS wireless channel conditions; as shown, there is no 5G signal power within the observed bandwidth now that the gNB is powered off. Upon correlating the baseline frequency bins, we see that the block diagonal structure is absent from all the correlation matrices (see Figure 8) which further supports the intuition that the 5G signal generated by the gNB is the cause of the block diagonal structures shown in Figure 5. Similarly, the LOS baseline PDF shown in Figure 8 is unimodal which further supports our intuition that the structure of the 5G signal is the cause of the bimodality exhibited by the LOS distributions in Figure 6.

In order to eliminate the effects of the wireless channel and any hardware idiosyncrasies, we also conducted simulations using the MATLAB 5G Toolbox [15] to replicate the 5G signal reception and verify our intuitions. Specifically, we created a 5G signal as represented by the spectrogram on the left hand side of Figure 9. The small vellow rectangles in the center of the bandwidth are Synchronization Signal Bursts (SSB), and are transmitted periodically as shown. Likewise, the larger rectangles in the lower portion of the bandwidth represent the Physical Downlink Control Channel (PDCCH) signals which are also transmitted periodically. We performed a similar correlation analysis (but averaging over a shorter time scale for convenience) using the PSDs created from the MATLAB 5G Toolbox and obtained the correlation matrix in the center of Figure 9. The small block in the middle of the correlation matrix (corresponding to frequencies in the center of the 5G signal bandwidth) and the larger block to its left (corresponding to frequencies in the lower portion of the 5G signal bandwidth) confirm our intuition that the block diagonal structure is caused by the structure of the 5G signal itself since these align with the spectrogram structure. We aren't saying the blocks in our field-test correlation matrices where caused by the SSB or PDDCH signals, but rather these serve as specific examples of general 5G signal structure which we argue is the root cause. Furthermore, the PDF of the frequency bin correlations (shown in the right hand portion of Figure 9) exhibits a bimodal structure which further bolsters the credibility of our our claim that the multimodal shape of the distribution is related to the pockets of high-correlation in the correlation matrices and, therefore, to the 5G signal characteristics.

Power Correlation Distributions for Spectrum Awareness

The practical benefit of analyzing the spectral correlation's probability distribution is that existing techniques for distribution analysis can be applied to spectral analysis. Metrics such as mean, variance, standard deviation, kurtosis, skewness, and modality can all be used to monitor the spectral utilization. Specifically, the multimodal structure of PDFs we displayed provide insight into the spectrum's utilization. A distinct multimodal structure indicates there are pockets of similar correlation values in the frequency bin correlation matrix; this in turn speaks to the clusterability of the signal's correlation. Furthermore, the existence of well-defined clusters speaks to the separability of the signals present in the observed bandwidth. The PDF modes obtained from signals with overlapping frequencies should be expected to be less distinct than those obtained from bandwidths containing signal with no overlapping frequencies. Thus, the modal structure of the probability distribution indicates the separability of the recorded signals.

Additionally, the PDF's mean plays an important part in determining the nature of the captured signal. Even if the distribution is unimodal, if the mean is high, this would seem to indicate that the signal present in the observed bandwidth (not necessarily only consisting of the signal from a single source, but possibly multiple sources) is structurally simplistic (i.e., it is not composed of distinct parts, unlike the spectrogram in Figure 9 which induces a bimodality).

Furthermore, while it is beyond the scope of this paper, kernel theory and clustering techniques could be used to shed additional light on the spectral usage characteristics.

## V. CONCLUSION AND FUTURE WORK

In this work we have presented a simple yet effective technique for spectrum awareness in commercial 5G networks. An analysis of the structure of the PSD correlation matrix, and more specifically the characteristics of the respective PDF distribution, provide insight into the 5G signal structure and the channel quality. We conducted an experimental study using AFRL's 5G test site in Stockbridge, New York in which we collected PSD measurements corresponding to three different wireless channel conditions (i.e., LOS, Edge, and

NLOS) at two different locations on site. An analysis of our results demonstrates that the frequency bin correlation matrices exhibit a unique block diagonal structure for the unobstructed wireless channel conditions, while they are much more uniform in obstructed instances. Likewise, we have demonstrated that the PDF distribution of the frequency bin correlations does not scale linearly upon moving from an unobstructed channel to a fully obstructed channel. Rather, a clear multimodality is present for the LOS wireless condition PDF, while this feature is completely absent from the NLOS distribution. Thus, the shape the distribution is changing with the wireless channel condition. Our findings indicate that the certain structural characteristics of the signal(s) generated by the transmitter(s) are detectable via our blind sensing approach in which we analyze the power correlation distributions.

We plan to extend this work in collaboration with AFRL in which we will further explore the probability distribution alterations that emerge under various wireless channel conditions, such as situations where many signals are present within the same portion of spectrum and/or when cellular devices are mobile. Additionally, we are interested to determine how quickly the block diagonal structure disappears from the LOS matrix as the distance is increased between the receiver and the gNB or as the gNB's signal power is decreased. Lastly, we hope to explore the use of kernel theory and clustering analysis on PSD data to better understand localized spectral utilization. With these questions in mind, we plan to continue this collaborative effort and integrate our findings with the Open RAN paradigm.

#### ACKNOWLEDGEMENT OF SUPPORT AND DISCLAIMER

This work has been funded in part by the National Science Foundation under grants CNS-2134973, ECCS-2229472, CNS-2312875 and ECCS-2329013, by the Air Force Office of Scientific Research under contract number FA9550-23-1-0261, by the Office of Naval Research under award number N00014-23-1-2221, and by the Air Force Research Laboratory via *Open Technology and Agility for Innovation (OTAFI)* under transaction number FA8750-21-9-9000 between SOSSEC, Inc. and the U.S. Government. The U.S. Government is authorized to reproduce and distribute reprints for Governmental purposes notwithstanding any copyright notation thereon. The views and conclusions contained herein are those of the authors and do not represent the official policies or endorsements, either expressed or implied, of Radiance Technologies, the U.S. Air Force, the U.S. Navy, or the U.S. Government.

#### REFERENCES

- L. Bonati, M. Polese, S. D'Oro, S. Basagni, and T. Melodia, "Open, programmable, and virtualized 5g networks: State-of-the-art and the road ahead," *Computer Networks*, vol. 182, p. 107516, 2020.
- [2] "Number of mobile devices worldwide 2020-2025 Statista statista.com," https://www.statista.com/statistics/245501/multiple-mobile-device-ownership-worldwide/, [Accessed 31-10-2023].
- [3] S. Haykin, D. J. Thomson, and J. H. Reed, "Spectrum sensing for cognitive radio," *Proceedings of the IEEE*, vol. 97, no. 5, pp. 849–877, 2009.

- [4] D. Chew and A. B. Cooper, "Spectrum sensing in interference and noise using deep learning," in 2020 54th Annual Conference on Information Sciences and Systems (CISS), 2020, pp. 1–6.
- [5] C. Liu, J. Wang, X. Liu, and Y.-C. Liang, "Deep cm-cnn for spectrum sensing in cognitive radio," *IEEE Journal on Selected Areas in Commu*nications, vol. 37, no. 10, pp. 2306–2321, 2019.
- [6] L. Zhang, M. Xiao, G. Wu, M. Alam, Y.-C. Liang, and S. Li, "A survey of advanced techniques for spectrum sharing in 5g networks," *IEEE Wireless Communications*, vol. 24, no. 5, pp. 44–51, 2017.
- [7] F. Restuccia, E. Blasch, A. Ashdown, J. Ashdown, and K. Turck, "3D-O-RAN: Dynamic data driven open radio access network systems," in MILCOM 2022-2022 IEEE Military Communications Conference (MILCOM). IEEE, 2022, pp. 19–24.
- [8] M. Polese, L. Bonati, S. D'oro, S. Basagni, and T. Melodia, "Understanding O-RAN: Architecture, interfaces, algorithms, security, and research challenges," *IEEE Communications Surveys & Tutorials*, 2023.
- [9] M. Polese, L. Bonati, S. D'Oro, S. Basagni, and T. Melodia, "Colo-RAN: Developing machine learning-based xapps for open ran closedloop control on programmable experimental platforms," *IEEE Transactions on Mobile Computing*, 2022.
- [10] E. Blasch, S. Ravela, and A. Aved, Handbook of Dynamic Data Driven Applications Systems. Springer, 2018.
- [11] E. Blasch, G. Seetharaman, and K. Reinhardt, "Dynamic Data Driven Applications System Concept for Information Fusion," *Procedia Computer Science*, vol. 18, pp. 1999–2007, 2013.
- [12] F. Darema, "Dynamic Data Driven Applications Systems: A New Paradigm for Application Simulations and Measurements," in *Interna*tional Conference on Computational Science. Springer, 2004, pp. 662– 669
- [13] E. Blasch, G. Seetharaman, and F. Darema, "Dynamic Data Driven Applications Systems (DDDAS) Modeling for Automatic Target Recognition," in *Automatic Target Recognition XXIII*, vol. 8744. International Society for Optics and Photonics, 2013, p. 87440J.
- [14] D. Uvaydov, S. D'Oro, F. Restuccia, and T. Melodia, "Deepsense: Fast wideband spectrum sensing through real-time in-the-loop deep learning," in *IEEE INFOCOM 2021 - IEEE Conference on Computer Communications*, 2021, pp. 1–10.
- [15] MathWorks, "5G Toolbox mathworks.com," https://www.mathworks.com/products/5g.html, [Accessed 02-02-2024].
- [16] "Stockbridge Research Site Griffiss Institute griffissinstitute.org," https://www.griffissinstitute.org/who-we-work-with/afrl/stockbridgeresearch-site, [Accessed 08-11-2023].
- [17] A. Ivanov, K. Tonchev, V. Poulkov, and A. Manolova, "Probabilistic spectrum sensing based on feature detection for 6g cognitive radio: A survey," *IEEE Access*, vol. 9, pp. 116 994–117 026, 2021.
- [18] Y. Arjoune and N. Kaabouch, "A comprehensive survey on spectrum sensing in cognitive radio networks: Recent advances, new challenges, and future research directions," *Sensors*, vol. 19, no. 1, 2019. [Online]. Available: https://www.mdpi.com/1424-8220/19/1/126
- [19] Y. Zhao, W. Fu, C. Zhou, and et al., "Energy correlation permutation algorithm of frequency-domain blind source separation based on frequency bins correction," Wireless Personal Communications, vol. 120, pp. 1753–1768, 2021.
- [20] G. Ding, F. Wu, Q. Wu, S. Tang, F. Song, A. V. Vasilakos, and T. A. Tsiftsis, "Robust online spectrum prediction with incomplete and corrupted historical observations," *IEEE Transactions on Vehicular Technology*, vol. 66, no. 9, pp. 8022–8036, 2017.
- [21] "Keysight Technologies (formerly Agilent) N9918A 30kHz-26.5GHz FieldFox handheld microwave combo analyzer — Electro Rent - Rental, New & Used Test Equipment — electrorent.com," https://www.electrorent.com/us/products/cable/site-masters-cabletesters/keysight-technologies/n9918a/01t1O000004TsAIQA0, [Accessed 09-05-2024].